JOURNAL OF SOLID STATE CHEMISTRY 110, 20–27 (1994)

Temperature-Dependent Structural Properties of *p*-Diiodobenzene: Neutron Diffraction and High-Resolution Solid State ^{13}C NMR Investigations

Xavier Alcobé

Serveis Cientifico-Tecnics, Universitat de Barcelona, 08028 Barcelona, Spain

Eugènia Estop

Departament de Geologia, Universitat Autonoma de Barcelona, 08193 Bellaterra, Spain

Abil E. Aliev and Kenneth D. M. Harris[1]

Department of Chemistry, University of St. Andrews, St. Andrews, Fife KY16 9ST, Scotland

Juan Rodríguez-Carvajal

Institut Laue Langevin, B.P. 156X, 38042 Grenoble Cedex, France

and

Jordi Rius

Institut de Ciencia de Materials (CSIC), 08193 Bellaterra, Spain

Received February 26, 1993; in revised form June 21, 1993; accepted July 7, 1993

p-diiodobenzene exists in two crystalline phases, both of which are orthorhombic, with space groups *Pbca* (α phase) and *Pccn* (β phase), respectively. The α phase is the stable form at ambient temperature, and a phase transition to the β phase occurs at ca. 326 K. This phase transition is associated with interesting hysteresis and metastability phenomena. From previous diffraction studies, the crystal structure of the α phase has been determined. In this work, we present a first structure determination of the β phase, from neutron powder diffraction data. It is shown that the structure of the β phase differs from the structure of the α phase by a change (ca. 46°) in the orientation of *half* of the molecules. This change in molecular orientation does not significantly alter the overall molecular packing arrangement (a fact consistent with the small change in lattice parameters and the small enthalpy change associated with the phase transition). The differences and similarities between crystal structures of the α and β phases are discussed in detail. The temperature-dependent structural properties of *p*-diiodobenzene have also been investigated by high-resolution solid state ^{13}C NMR spectroscopy. Detailed results from these investigations are reported and discussed in the light of the results from the neutron diffraction studies. Furthermore, in view of the fact that only rather small structural differences exist between the α and β phases of *p*-diiodobenzene, our results have wider implications from the viewpoint of assessing the scope of solid state NMR spectroscopy as a technique for probing *minor* changes in structural properties of crystalline organic solids.

1. INTRODUCTION

p-dihalogenobenzenes are of considerable interest at present since many of them are known to form isostructural binary molecular alloys $(W(C_6H_4)X)_{1-\delta}(Y(C_6H_4)Z)_\delta$ ($0 < \delta < 1$; W, X, Y, and Z represent halogen functional groups) (1, 2) which have potential applications as materials for energy storage devices (3, 4). The temperature–composition phase diagrams of a wide range of these materials have been determined (5–7).

Many of the "pure" crystalline materials (i.e., those with $\delta = 0$) themselves have interesting solid state properties, and in this paper we consider the temperature dependence of the structural properties of *p*-diiodobenzene ($I(C_6H_4)I$; denoted *p*-DIB). This material is known (8) to exist in two crystalline phases, both of which are orthorhombic, with space groups *Pbca* (α phase) and *Pccn* (β phase), respectively. When *p*-DIB is crystallized from

[1] To whom correspondence should be addressed at Department of Chemistry, University College London, 20 Gordon Street, London WC1H OAJ, England.

0022-4596/94 $6.00

acetone at room temperature, a monophasic sample of the α phase is obtained. On warming this sample, a phase transition to the β phase occurs at ca. 326 K. This transition is associated with interesting hysteresis and metastability phenomena which have been studied by neutron diffraction (8), X-ray diffraction (9), optical techniques (9), differential scanning calorimetry (10), Raman spectroscopy (11), infrared spectroscopy (12), photoconductivity (13), and nuclear quadrupole resonance spectroscopy (14). Previous X-ray diffraction studies have succeeded in determining the crystal structure of the α phase at room temperature (15, 16).

In the previous neutron diffraction study (8), powder diffractograms were recorded at several different temperatures from 1.5 to 313 K for the α phase, and from 333 to 383 K for the β phase. The Rietveld profile refinement method (as implemented by Wiles and Young (17)) was used, without imposing any structural constraints, for structure refinement of both the α and β phases. In spite of good profile fits obtained for both phases (R_p = 5.2, R_{wp} = 7.0, Bragg R-factor = 3.8 at 1.5 K; R_p = 3.9, R_{wp} = 5.4, Bragg R-factor = 7.4 at 383 K), only the results obtained at 1.5 and 208 K corresponded to plausible geometries for the *p*-DIB molecule. The molecular geometries obtained in refinements from the data at 238 to 383 K were strongly deformed from plausible geometries. The same situation was encountered during the unconstrained crystal structure refinements of *p*-dichlorobenzene, *p*-dibromobenzene, and some of their molecular alloys from neutron powder diffraction data recorded at 293 K (18). Structure determination from single crystal X-ray diffraction data, on the other hand, gave a molecule with symmetry close to *mmm*.

In part, the lack of success in the structure refinement from the powder diffraction data is a consequence of the rapid decrease in the intensity of neutron powder diffraction peaks at higher scattering angles on increasing the temperature (see Fig. 1). Nevertheless, these previous neutron diffraction studies have allowed the following information to be determined: (1) the structure of the α phase at low temperature (1.5 K), (2) the lattice parameters and space group of the β phase, and (3) the temperature dependence of the lattice parameters for the α and β phases, and the manner in which these parameters change at the phase transition.

In view of the problems encountered in the unconstrained structure refinements at higher temperatures, rigid body refinement calculations were carried out, assuming the molecular geometry to be the same as that obtained in the unconstrained refinement at 1.5 K. In this paper, we report the results of these structure refinement calculations for the α phase at 298 K and for the β phase at 333 K.

In addition, high-resolution solid state ^{13}C NMR spectroscopy has been used in order to investigate and understand alterations in local structural properties associated with the phase transition in *p*-DIB; the results from these investigations are reported here.

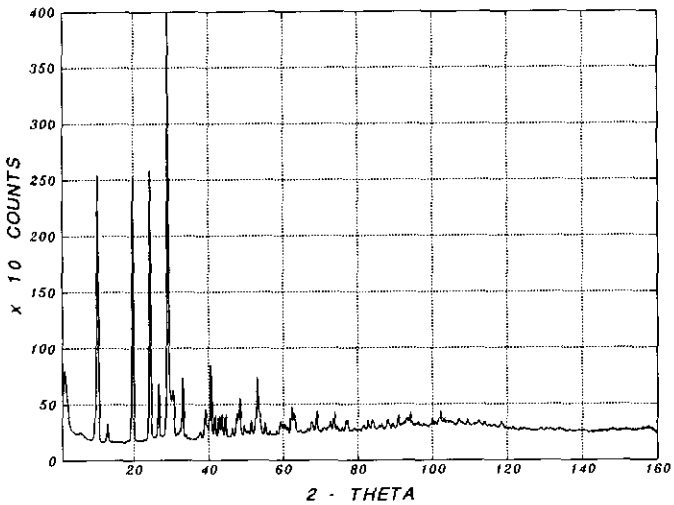

FIG. 1. Neutron powder diffractogram of the β phase of *p*-DIB-d_4 recorded at 333 K.

2. EXPERIMENTAL AND COMPUTATIONAL DETAILS

The fully deuterated sample of *p*-DIB (denoted *p*-DIB-d_4) used for neutron powder diffraction experiments was prepared by treatment of benzene-d_6 (99.6 at.% D, CEA) with iodine and HIO_3/H_2SO_4 in $AcOH/H_2O$, using the method described for the synthesis of *p*-DIB from benzene (19). The sample was purified by recrystallization from a MeOH/AcOEt solution. The purity of the sample was assessed by analysis of the melting signal shape in its differential scanning calorigram (20). The sample of *p*-DIB-d_4 prepared in this way was shown by powder X-ray diffraction to be a mixture of the α and β phases at room temperature (β phase metastable). To obtain a monophasic sample of the α phase at room temperature, the sample was immersed in liquid nitrogen for ca. 90 min before being returned to room temperature. This sample remained monophasic α phase until taken above the phase transition temperature, and became monophasic β phase above this temperature.

Neutron powder diffractograms were recorded on the high-resolution diffractometer D2B at the Institut Laue-Langevin, Grenoble, with wavelength λ = 1.5946 Å and step scan increment $\Delta(2\theta)$ = 0.05°.

Rigid-body Rietveld refinement calculations were carried out using a version of the RIBOLS program (21) adapted to neutron powder diffraction data. Only the 2θ interval (15–59°) containing strong peaks was considered; over this restricted 2θ range, the peak shape and linewidth

TABLE 1

Details of the Rigid-Body Rietveld Refinement of the α Phase of p-DIB-d_4 from Neutron Powder Diffraction Data Collected at 298 K

Range of 2θ (°)	15–58
Space group	*Pbca*
Z	4
Lattice parameters (Å):	
a	17.000
b	7.323
c	6.168
Zero shift in 2θ (°)	0.22
Pseudo-Voigt profile function	0.1 Lorentzian, 0.9 Gaussian
Preferred orientation parameter G_1	1.3
Number of refined structural parameters	4
Estimated standard deviations (σ) of Euler angles defining the molecular orientation (°)	
$\sigma(\psi_1)$	0.15
$\sigma(\psi_2)$	0.39
$\sigma(\psi_3)$	0.28
$B_{overall}$ (Å^2)	4.5(2)
Number of refined profile parameters	2
Scale factor c	0.72(3)
FWHM in 2θ (°)	0.50(2)
Number of observed reflections	89
R_{wp} (%)	12.1

TABLE 2

Details of the Rigid-Body Rietveld Refinement of the β Phase of p-DIB-d_4 from Neutron Powder Diffraction Data Collected at 333 K

Range of 2θ (°)	15–59
Space group	*Pccn*
Z	4
Lattice parameters (Å):	
a	17.092
b	7.461
c	6.154
Zero shift in 2θ (°)	0.23
Pseudo-Voigt profile function	0.1 Lorentzian, 0.9 Gaussian
Preferred orientation parameter G_1	1.3
Number of refined structural parameters	4
Estimated standard deviations (σ) of Euler angles defining the molecular orientation (°)	
$\sigma(\psi_1)$	0.28
$\sigma(\psi_2)$	0.52
$\sigma(\psi_3)$	0.48
$B_{overall}$ (Å^2)	5.8(4)
Number of refined profile parameters	2
Scale factor c	0.68(3)
FWHM in 2θ (°)	0.48(2)
Number of observed reflections	92
R_{wp} (%)	13.1

(FWHM) could be assumed to be constant. This strategy for profile refinement has been applied successfully in other cases (22). Relevant parameters relating to the refinement calculations of the α and β phases of p-DIB-d_4 are given in Tables 1 and 2, respectively.

As discussed in Section 1, the p-DIB molecule was considered as a rigid body in all structure refinement calculations. In the refinements from the diffractograms recorded at 298 and 333 K, the molecular geometry (see Table 3) and the initial orientation of the molecule relative to the unit cell axes were taken to be the same as those determined in the unconstrained refinement from the diffractogram recorded at 1.5 K (see Section 1). In the α phase (space group *Pbca*) it is known that the center of symmetry of the molecules lies on a crystallographic center of symmetry; consequently, only the orientation of the molecule needs to be refined, and the position of the center of the molecule was fixed during the refinements. The similarity of the lattice parameters for the α and β phases, together with structural and symmetry considerations (space group *Pccn* for the β phase), leads us to assume that the center of symmetry of the molecule in the β phase is also located on a crystallographic center of symmetry.

The crystallites of the powder samples used in this work had a plate-like habit, with the reciprocal lattice vector (100) normal to the plane of the crystallites. To take into

TABLE 3

Bond Distances and Bond Angles for the Rigid-Body Molecular Model Used in the Structure Refinement Calculations Discussed in the Text

Bond distance (Å)		Bond angle (°)	
I1–C1	2.096	I1–C1–C6	118.8
C1–C2	1.385	I1–C1–C2	120.9
C1–C6	1.400	C2–C1–C6	120.3
C2–C3	1.391	C1–C2–C3	120.1
C2–D2	1.096	C2–C3–C4	119.5
C3–D3	1.091	C1–C2–D2	119.9
		C3–C2–D2	120.0
		C2–C3–D3	120.2
		D3–C3–C4	120.3

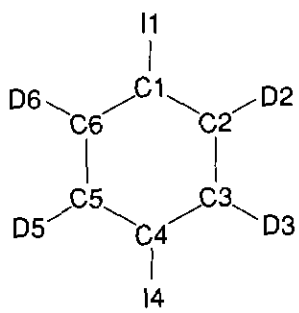

Note. Only data for the asymmetric unit (which comprises half of the molecule) are included.

account the effect of preferred orientation, the measured intensities were corrected by the factor (23) $(G_1^2 \cos^2\alpha + (\sin^2\alpha)/G_1)^{-1.5}$, where α is the acute angle between the scattering vector and the normal to the plane of the crystallites, and G_1 is a refinable parameter.

For the structure refinements of the α phase (see Table 1) and the β phase (see Table 2), the following parameters were taken from the previous unconstrained refinements at 298 and 333 K, respectively (8): the lattice parameters, the Gaussian component of the pseudo-Voigt profile function, and the G_1 parameter. The starting value for the overall temperature factor B was taken as the average of the isotropic temperature factors obtained for the six atoms in the asymmetric unit in the unconstrained refinement, and the starting value of the FWHM was taken as the average of the actual values in the 2θ range 15–59°. Only six parameters were refined: three parameters defining the orientation of the rigid molecule (Euler angles), the overall temperature factor B, the scale factor, and the FWHM.

The goodness-of-fit index R_{wp} is defined as

$$R_{wp} = \left(\frac{\Sigma w_i[y_i(\text{obs}) - y_i(\text{calc})]^2}{\Sigma w_i[y_i(\text{obs})]^2}\right)^{1/2},$$

where y_i(obs) is the net intensity at data point i of the powder diffraction profile (note that RIBOLS only takes into account data points i which represent part of a reflection), y_i(calc) is the calculated intensity at data point i, and w_i is the weighting factor associated with data point i.

High-resolution solid state ^{13}C NMR spectra were recorded at 125.76 MHz on a Bruker MSL500 spectrometer using a standard Bruker MAS probe with double-bearing rotation mechanism. The samples were studied as powders in zirconia rotors (4-mm external diameter) and subjected to magic angle sample spinning (MAS) at 8 kHz, with stability better than ca. ± 10 Hz; faster spinning did not improve the quality of the spectra. In the case of the sample of p-DIB with natural isotopic abundances (denoted p-DIB-h_4), the ^1H–^{13}C cross polarization (CP) method was employed, with the spectrum recorded under conditions of high-power ^1H decoupling. The ^1H radiofrequency field strength used in this decoupling corresponded to a ^1H 90° pulse width of ca. 5μs. ^{13}C chemical shifts are given relative to tetramethylsilane, established via the use of adamantane (methine carbon signal at 29.47 ppm) as an external standard. In the case of p-DIB-d_4, a "single pulse" sequence was used to record the ^{13}C NMR spectra, with the spectrum recorded under conditions of high-power ^1H decoupling. The digital resolution in all ^{13}C NMR spectra was ca. 0.5 Hz, and the accuracy of the temperature measurements was ca. ±2 K. The sample of p-DIB-h_4 (Aldrich) used in this work was shown (at room temperature) to be a monophasic sample of the α phase.

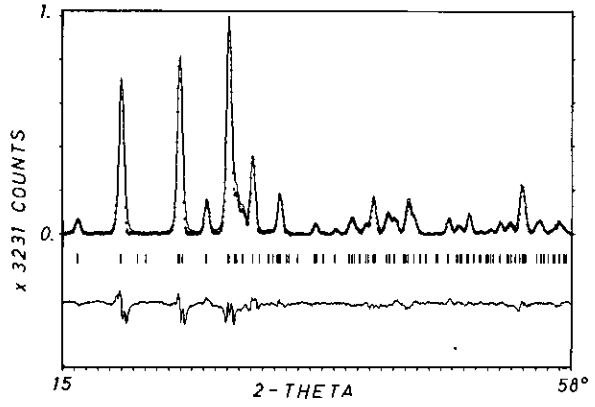

FIG. 2. Measured (+) and calculated (solid line) neutron powder diffractograms, and the difference between the two (below), for the refinement of the α phase of p-DIB-d_4 at 298 K. The positions of reflections are marked.

3. RESULTS AND DISCUSSION

The final values for the refined parameters, together with the R_{wp} factors, are given in Table 1 (α phase) and Table 2 (β phase). Figures 2 and 3 show the good agreement between the observed and calculated powder diffractograms at 298 K (α phase) and 333 K (β phase), respectively. The final fractional atomic coordinates for the α phase at 298 K and for the β phase at 333 K are given in Table 4.

Considering the α phase, the crystal structure reported here at 298 K is essentially the same as the room temperature structure reported previously (16). The only minor differences concern the lattice parameter a (which differs by 0.06 Å) and the orientation of the molecular plane (which differs by 4°).

The final refined structures of the α phase (298 K) and

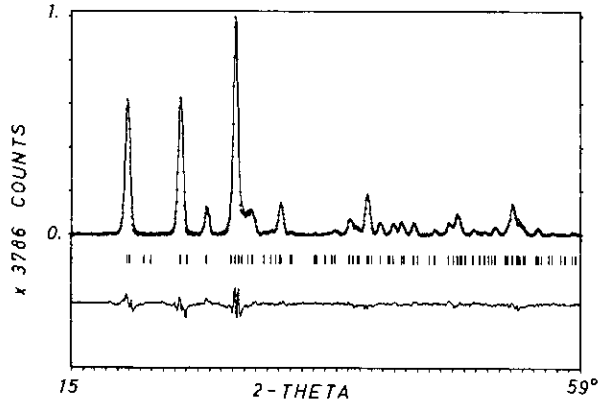

FIG. 3. Measured (+) and calculated (solid line) neutron powder diffractograms, and the difference between the two (below), for the refinement of the β phase of p-DIB-d_4 at 333 K. The positions of reflections are marked.

TABLE 4
Fractional Atomic Coordinates for the α phase (298 K) and β phase (333 K) of p-DIB-d_4

Atom	x/a	y/b	z/c
		α phase (298 K)	
I1	0.1713(6)	0.0373(14)	0.3067(17)
C1	0.0691(2)	0.0180(6)	0.1183(7)
C2	0.0717(2)	−0.0525(6)	−0.0900(7)
C3	0.0027(2)	−0.0728(6)	−0.2090(7)
D2	0.1279(4)	−0.0962(10)	−0.1592(12)
D3	0.0045(4)	−0.1313(10)	−0.3715(12)
		β phase (333 K)	
I1	0.1694(9)	0.0392(21)	0.3111(25)
C1	0.0683(4)	0.0187(8)	0.1200(10)
C2	0.0715(4)	−0.0529(8)	−0.0875(10)
C3	0.0033(4)	−0.0738(8)	−0.2082(10)
D2	0.1277(7)	−0.0969(15)	−0.1547(18)
D3	0.0056(7)	−0.1331(15)	−0.3700(18)

Note. Figures in parentheses represent the estimated standard deviation in the last quoted digit.

β phase (333 K) of p-DIB-d_4 are shown in Figs. 4 and 5, respectively. The observed differences between lattice parameters for these phases (see Tables 1 and 2) are consistent with the expansion along a and b, and the contraction along c, which are already known (8) to be associated with the phase transition from the α phase to the β phase. These differences in the lattice parameters are comparatively small. Structurally, the differences between the α and β phases are small but significant. In each structure, the p-DIB molecules are located in "layers" parallel to (100) at $x \approx 0$ and $x \approx 1/2$. The change in space group from *Pbca* (α phase) to *Pccn* (β phase) can be described geometrically by a translation of the molecules in the layer at $x \approx 1/2$ by the vector $(1/2)\mathbf{b} + (1/2)\mathbf{c}$. Essentially, this corresponds to a change in the orientation of the

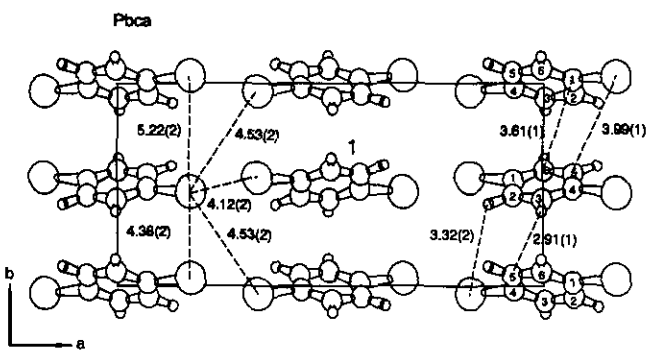

FIG. 4. Crystal structure of the α phase of p-DIB-d_4 at 298 K, viewed along the **c** axis. The shortest C . . . D, I . . . D, C . . . C, and I . . . C intermolecular distances are indicated. The five shortest I . . . I distances for a central iodine atom are also indicated.

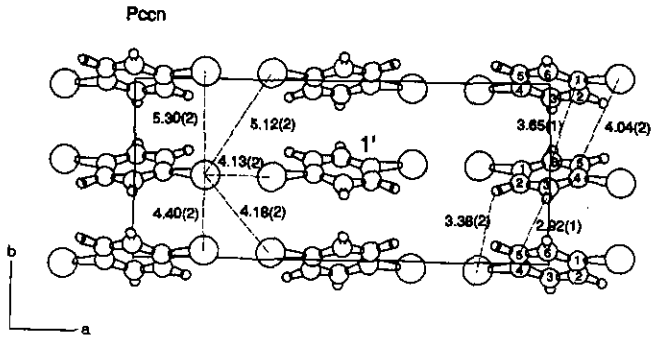

FIG. 5. Crystal structure of the β phase of p-DIB-d_4 at 333 K, viewed along the **c** axis. The shortest C . . . D, I . . . D, C . . . C, and I . . . C intermolecular distances are indicated. The five shortest I . . . I distances for a central iodine atom are also indicated.

molecules in this layer by ±46° when passing from the α phase to the β phase (compare the orientations of molecule 1 in Fig. 4 and molecule 1′ in Fig. 5). Consistent with the description of the phase transition as arising from the translation of one layer of molecules, the intermolecular "contacts" *within* each layer are very similar in the α and β phases. On the other hand, the intermolecular "contacts" *between* adjacent layers differ substantially between the α and β phases.

The structural similarities and differences between the α and β phases can be discussed through an analysis of the intermolecular, interatomic distances (see Table 5 and also Fig. 4 (α phase) and Fig. 5 (β phase)). First, we note that most of the short intermolecular contacts (defined as those interatomic distances that are within a few percent of the sum of the van der Waals radii of the corresponding atoms) are located *within* individual layers. The shortest intermolecular contacts of the types C . . . D, I . . . D, C . . . C, and I . . . C are always located *within* individual layers. For I . . . I contacts, however, the shortest distances are established *between* adjacent layers. Second, none of the intermolecular intralayer distances changes significantly at the phase transition (the small differences observed are consistent with the changes of unit cell parameters associated with the phase transition (vide supra)). In contrast, the intermolecular interlayer distances differ substantially between the α and β phases, as a consequence of the fact that the molecules in adjacent layers are related by different symmetry operations. In the α phase, there is only one short I . . . I interlayer contact (4.12(2) Å), whereas there are two short I . . . I interlayer contacts in the β phase (4.13(2) and 4.18(2) Å).

In each phase, there are two crystallographically inequivalent C–H (actually C–D) carbon atoms (C2 and C3 in Table 3), whereas there is only one crystallographically distinct C–I carbon atom. The intralayer environ-

TABLE 5

Observed Intermolecular, Interatomic Distances for the α and β phases of *p*-DIB-d_4, and Comparison with Corresponding Distances Calculated by the Sum of van der Waals Radii

	α Phase (298 K)			β Phase (333 K)		
Calculated distance (Å)	Interaction	Observed distance (Å)		Interaction	Observed distance (Å)	
		Intra-layer	Inter-layer		Intra-layer	Inter-layer
2.34	D3 . . . D6	2.50(1) *c*		D3 . . . D6	2.56(2) *c*	
2.97	C5 . . . D3	sh.c. 2.91(1) $2_1 \| b$		C5 . . . D3	sh.c. 2.92(1) $2_1 \| b$	
	C6 . . . D3	sh.c. 2.99(1) *c*		C6 . . . D3	sh.c. 3.02(1) *c*	
	C6 . . . D3	sh.c. 3.01(1) $2_1 \| b$		C6 . . . D3	sh.c. 3.02(1) $2_1 \| b$	
3.27	I4 . . . D2	sh.c. 3.32(2) $2_1 \| b$		I4 . . . D2	sh.c. 3.38(2) $2_1 \| b$	
	I1 . . . D2		3.45(2) $2_1 \| c$			
3.60	C1 . . . C6	sh.c. 3.61(1) $2_1 \| b$		C1 . . . C6	sh.c. 3.65(1) $2_1 \| b$	
	C3 . . . C3	sh.c. 3.70(1) $2_1 \| b$		C3 . . . C3	sh.c. 3.77(1) $2_1 \| b$	
	C3 . . . C6	sh.c. 3.75(1) *c*		C3 . . . C6	sh.c. 3.76(1) *c*	
3.90	I1 . . . C5	sh.c. 3.99(1) $2_1 \| b$		I1 . . . C5	sh.c. 4.04(2) $2_1 \| b$	
	I1 . . . C2	4.14(1) *c*		I1 . . . C2	4.12(2) *c*	
4.20	I4 . . . I4		sh.c. 4.12(2) $2_1 \| c$	I4 . . . I1		sh.c. 4.13(2) $2_1 \| a$
	I4 . . . I1		4.53(2) $2_1 \| a$	I4 . . . I4		sh.c. 4.18(2) $2 \| c$
	I4 . . . I1		4.53(2) $2_1 \| a$	I4 . . . I4		5.12(2) $2 \| c$
	I4 . . . I1	sh.c. 4.38(2) $2_1 \| b$		I4 . . . I1	sh.c. 4.40(2) $2_1 \| b$	
	I4 . . . I1	5.22(2) $2_1 \| b$		I4 . . . I1	5.30(2) $2_1 \| b$	
	I4 . . . I4	6.17(1) $\pm c$		I4 . . . I4	6.15(1) $\pm c$	

Note. Definitions of the atom numbering are given in Table 3 and Figs. 4 and 5. The abbreviation sh.c. indicates "short contact" (as defined in the text). For all the types of interaction except I . . . I, only the shortest distances are given. For I . . . I interactions, the distances for the six iodines closest to a central iodine (I4) are given. The symbols *c*, $2_1 \| a$, $2_1 \| b$, $2_1 \| c$, $2 \| c$ indicate, respectively, interatomic distances between two molecules related by a *c* translation, by a 2_1 axis parallel to *a*, *b*, or *c*, or by a 2 axis parallel to *c*.

ment for each of these carbons is substantially the same in the α and β phases (see Table 5 and Figs. 4 and 5), and the principal environmental differences between the carbon atoms of the α and β phases are concerned with interlayer interactions. Since the "interface" between adjacent layers involves primarily the interaction between C–I groups rather than C–D groups (which are located within the "interior" of each layer), some short intermolecular contacts (the interlayer contacts) involving the C–I groups are considerably different in the α and β phases, whereas none of the short intermolecular contacts (all of which are intralayer contacts) involving the C–D groups are significantly different in the α and β phases. All interlayer distances involving the C–D groups are long range. These structural features concerning the environments of the carbon atoms are relevant in connection with the ^{13}C NMR results discussed below.

Our high-resolution solid state ^{13}C NMR investigations of *p*-DIB-h_4 corroborate the main structural conclusion, discussed above, that there are important (although small) alterations in structural properties with variation of temperature. Figure 6 shows high-resolution solid state ^{13}C NMR spectra of a sample of *p*-DIB-h_4 recorded on increasing the temperature from 295 to 363 K. The sample used at the beginning of these experiments was a monophasic sample of the α phase of *p*-DIB-h_4.

The peaks at ca. 139.4 and 141.5 ppm in the 295 K spectrum (Fig. 6) are assigned to the two crystallographically inequivalent C–H carbon environments in the α phase. There is a single broad line at ca. 99.5 ppm due to the C–I carbons. Above the phase transition temperature (ca. 326 K), there is a single line at ca. 140.5 ppm representing the C–H carbons of the β phase; the resonances due to the two crystallographically inequivalent carbon environments of this type are unresolved. There is a single broad line at ca. 97.5 ppm due to the C–I carbon environment. The isotropic chemical shift of the C–I carbons is clearly more sensitive to the phase of *p*-DIB than the isotropic chemical shift of the C–H carbons. This fact is consistent with the conclusions from the neutron diffraction results discussed above that the local environment of the C–I carbons is affected far more significantly as a consequence of the transition from the α phase to the β phase than is the local environment of the C–H carbons.

^{13}C NMR spectra recorded on raising the temperature of *p*-DIB-d_4 across the phase transition temperature from the α phase to the β phase exhibit the same behavior discussed above for *p*-DIB-h_4.

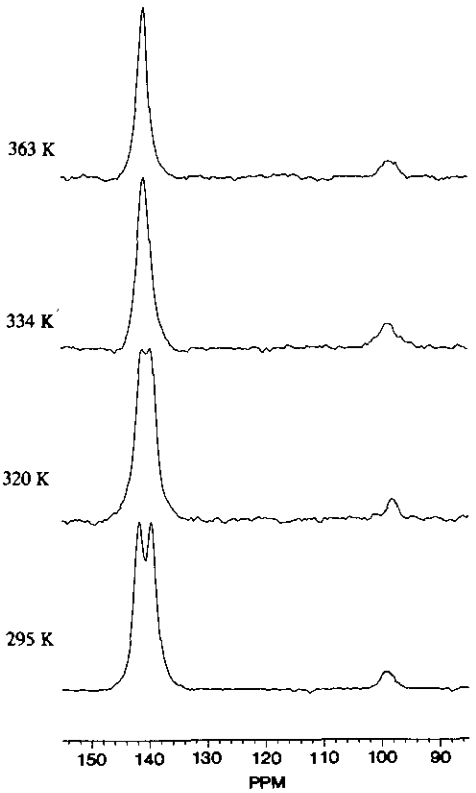

FIG. 6. ^{13}C NMR spectra of p-DIB-h_4 recorded at 125.76 MHz using the ^{13}C CPMAS method (τ_{cp} = 0.5 ms; $\nu_r \approx 8$ kHz; recycle delay = 30–60 sec) with high power ^1H decoupling applied during acquisition.

4. CONCLUDING REMARKS

The work reported here represents the first successful determination of the crystal structure of the β phase of p-DIB, and thus, in combination with the previously known crystal structure of the α phase, allows a structural rationalization of the phase transition in this system. The fact that the transition is associated with only a rather minor structural change (i.e., a change in orientation of the molecules in every second "layer") is consistent with the small change in lattice parameters and the small enthalpy change (ca. 198 $Jmole^{-1}$) at the transition. At present, however, several important issues relating to this transition are not yet satisfactorily understood, particularly in relation to the hysteresis associated with the transition and in relation to the existence of metastable phases. It is also relevant to consider the small but subtle effects that deuteration may confer upon the system with regard to the phase transition behavior. For example, it has been noted (24) that when a monophasic sample of the β phase of p-DIB-d_4 is cooled to room temperature, some amount of the β phase remains (as a metastable phase), whereas when a monophasic sample of the β phase of p-DIB-h_4 is cooled to room temperature, a monophasic sample of the α is obtained.

It is also relevant to note the success of the high-resolution solid state ^{13}C NMR experiments in providing meaningful information on the local structural changes associated with the phase transition in p-DIB. It is already well established (25, 26) that this technique can successfully distinguish different crystalline polymorphs of a given molecular species when there are major differences in crystal structure between these polymorphs; the results reported here demonstrate that this technique can also provide important structural insights in those cases (exemplified by the α and β phases of p-DIB) for which there are only minor structural differences between the crystalline phases in question.

ACKNOWLEDGMENTS

We are grateful to Dr A. Alvarez-Larena for synthesizing the sample of p-DIB-d_4 used in this work. Financial support from CAICYT (project no. PB89-0281-C03-03), the Royal Society (postdoctoral Fellowship to A.E.A.), and the S.E.R.C. (general support to K.D.M.H.) is gratefully acknowledged.

REFERENCES

1. M. T. Calvet, M. A. Cuevas-Diarte, Y. Haget, P. R. Van Der Linde, and H. A. J. Oonk, *CALPHAD: Comput. Coupling Phase Diagrams Thermochem.* **15,** 225 (1991).
2. L. Bonpunt, R. Courchinoux, Y. Haget, E. Estop, T. Calvet, M. A. Cuevas-Diarte, and M. Labrador, *J. Appl. Crystallogr.* **24,** 164 (1991).
3. M. Labrador, thesis. University of Barcelona, 1990.
4. D. Mondieig, Y. Haget, M. Labrador, M. A. Cuevas-Diarte, P. R. Van Der Linde, and H. A. J. Oonk, *Mater. Res. Bull.* **26,** 1091 (1991).
5. Y. Haget, J. R. Housty, A. Maiga, L. Bonpunt, N. B. Chanh, M. Cuevas, and E. Estop, *J. Chim. Phys.–Chim. Biol.* **81,** 197 (1984).
6. T. Calvet, thesis. University of Barcelona, 1990.
7. T. Calvet, X. Alcobe, E. Tauler, M. A. Cuevas-Diarte, E. Estop, D. Mondieig, and Y. Haget, *Powder Diffr.* **6,** 85 (1991).
8. X. Alcobe, E. Estop, J. Rodriguez, A. Alvarez, M. Labrador, and T. Calvet, *in* "Abstracts from Powder Diffraction, Satellite Meeting of the XVth I.U.Cr. Congress," p. 165 (1990).
9. L. J. Soltzberg, S. M. Cannon, Y.W. Ho, E. C. Armstrong, and S. J. Bobrowski, *J. Chem. Phys.* **75,** 859 (1981).
10. X. Alcobe, E. Estop, M. A. Cuevas-Diarte, and Y. Haget, XXII Reunión Bienal de la Real Sociedad Española de Química **4,** 60 (1988).
11. S. P. Cramer and B. Hudson, *J. Chem. Phys.* **64,** 1140 (1976).
12. B. P. Clayman, B. Farnworth, and R. W. Ward, *J. Chem. Phys.* **68,** 4930 (1978).
13. L. M. Schwartz, H. G. Ingersoll, and J. F. Hornig, *Mol. Cryst.* **2,** 379 (1967).
14. A. D. McDonald and S. Hacobian, *J. Mol. Struct.* **111,** 109 (1983).
15. Y. T. Struchkov and L. Dun-Chai, *Izv. Akad. Nauk SSSR, Ser. Khim.* **12,** 2095 (1959).
16. A. Hinchliffe, R. W. Munn, R. G. Pritchard, and C. J. Spicer, *J. Mol. Struct.* **130,** 93 (1985).
17. D. B. Wiles and R. A. Young, *J. Appl. Crystallogr.* **15,** 430 (1982).

18. A. Belaaraj, thesis. University of Barcelona, 1992.
19. H. O. Wirth, O. Königstein, and W. Kern, *Ann. Chem.* **634,** 84 (1960).
20. T. Calvet, E. Tauler, M. A. Cuevas-Diarte, J. R. Housty, D. Mondieig, Y. Haget, and J. C. Van Miltenburg, *Thermochim. Acta* **204,** 271 (1992).
21. J. Rius, "Ribols—A program for the rigid-body Rietveld least-squares refinement." Institut de Ciencia de Materials de Barcelona, Spain.
22. J. Rius, C. Miravitlles, E. Molins, M. Crespo, and J. Veciana, *Mol. Cryst. Liq. Cryst.* **187,** 155 (1990).
23. W. A. Dollase, *J. Appl. Crystallogr.* **19,** 267 (1986).
24. X. Alcobe and E. Estop, unpublished X-ray diffraction results.
25. G. E. Balimann, C. J. Groombridge, R. K. Harris, K. J. Packer, B. J. Say, and S. F. Tanner, *Philos. Trans. R. Soc. London, Ser. A***299,** 643, (1981).
26. K. D. M. Harris and J. M. Thomas, *J. Solid State Chem.* **93,** 197, (1991).